J|A|C|S
ARTICLES

Published on Web 06/20/2008

Formation and Reactivity of a Persistent Radical in a Dinuclear Molybdenum Complex

Aaron M. Appel,[†] Suh-Jane Lee,[†] James A. Franz,*[,†] Daniel L. DuBois,[†] M. Rakowski DuBois,[†] Jerome C. Birnbaum,[†] and Brendan Twamley[‡]

Pacific Northwest National Laboratory, P.O. Box 999, Richland, Washington 99352, and Department of Chemistry, University of Idaho, Moscow, Idaho 83844-2343

Received October 23, 2007; Revised Manuscript Received April 16, 2008; E-mail: james.franz@pnl.gov

Abstract: The reactivity of the S−H bond in Cp*Mo(μ-S)$_2$(μ-SMe)(μ-SH)MoCp* (**S_4MeH**) has been explored by determination of kinetics of hydrogen atom abstraction to form the radical Cp*Mo(μ-S)$_3$(μ-SMe)MoCp* (**S_4Me•**), as well as reaction of hydrogen with the radical-dimer equilibrium to reform the S−H complex. From the temperature dependent rate data for the abstraction of hydrogen atom by benzyl radical, $\Delta H^{\ddagger}$ and $\Delta S^{\ddagger}$ were determined to be 1.54 ± 0.25 kcal/mol and −25.5 ± 0.8 cal/mol K, respectively, giving $k_{abs} = 1.3 \times 10^6$ M^{-1} s^{-1} at 25 °C. In steady state abstraction kinetic experiments, the exclusive radical termination product of the Mo_2S_4 core was found to be the benzyl cross-termination product, Cp*Mo(μ-S)$_2$(μ-SMe)(μ-SBz)MoCp* (**S_4MeBz**), consistent with the Fischer−Ingold persistent radical effect. **S_4Me•** was found to reversibly dimerize by formation of a weak bridging disulfide bond to form the tetranuclear complex (Cp*Mo(μ-S)$_2$(μ-SMe)MoCp*)$_2$(μ-S$_2$) (**(S_4Me)$_2$**). The radical-dimer equilibrium constant has been determined to be $5.7 \times 10^4 \pm 2.1 \times 10^4$ M^{-1} from EPR data. The rate constant for dissociation of the dimer was found to be 1.1×10^3 s^{-1} at 25 °C, based on variable temperature ^{1}H NMR data. The rate constant for dimerization of the radical has been estimated to be 6.5×10^7 M^{-1} s^{-1} in toluene at room temperature, based on the dimer dissociation rate constant and the equilibrium constant for dimerization. Structures are presented for **(S_4Me)$_2$**, **S_4MeBz**, and the cationic Cp*Mo(μ-S$_2$)(μ-S)(μ-SMe)MoCp*(OTf) (**S_4Me$^+$**), a precursor of the radical and the alkylated derivatives. Evidence for a radical addition/elimination pathway at an Mo_2S_4 core is presented.

Introduction

Homogenous molybdenum sulfide complexes have been widely studied due to their importance in understanding fundamental reaction channels available to molybdenum sulfide based hydrodesulfurization (HDS) catalysts[1–3] and the important role that molybdenum sulfide complexes play in enzymatic reactions.[3–5] $Cp_2Mo_2S_4$ complexes have been extensively studied because of their ability to activate hydrogen and undergo bond-forming reactions with a variety of hydrocarbons.[6–15] In addition to the many examples of hydrogen utilization reactions, these complexes can also be used for the production of hydrogen, as demonstrated in our report of $(CpMoS)_2(S_2CH_2)$ as an electrocatalyst for hydrogen production at low overpotentials.[16] Studying the formation and cleavage of S−H bonds in Mo_2S_4-based complexes is central to understanding the wide range of observed reactivities.

Investigations of hydrogen atom transfer kinetics and thermodynamics are also important for hydrogenation,[17–20] chain transfer polymerization,[21–25] and initiation of other radical

† Pacific Northwest National Laboratory.
‡ University of Idaho.

(1) Grange, P.; Vanhaeren, X. *Catal. Today* **1997**, *36*, 375–391.
(2) Bianchini, C.; Meli, A. *Acc. Chem. Res.* **1998**, *31*, 109–116.
(3) Donahue, J. P. *Chem. Rev.* **2006**, *106*, 4747–4783.
(4) Hille, R. *Chem. Rev.* **1996**, *96*, 2757–2816.
(5) Brondino, C. D.; Rivas, M. G.; Romao, M. J.; Moura, J. J. G.; Moura, I. *Acc. Chem. Res.* **2006**, *39*, 788–796.
(6) Rakowski Dubois, M.; Haltiwanger, R. C.; Miller, D. J.; Glatzmaier, G. *J. Am. Chem. Soc.* **1979**, *101*, 5245–5252.
(7) Rakowski Dubois, M.; Vanderveer, M. C.; Dubois, D. L.; Haltiwanger, R. C.; Miller, W. K. *J. Am. Chem. Soc.* **1980**, *102*, 7456–7461.
(8) Rakowski Dubois, M.; Dubois, D. L.; Vanderveer, M. C.; Haltiwanger, R. C. *Inorg. Chem.* **1981**, *20*, 3064–3071.
(9) Brunner, H.; Meier, W.; Wachter, J.; Guggolz, E.; Zahn, T.; Ziegler, M. L. *Organometallics* **1982**, *1*, 1107–1113.
(10) Curtis, M. D.; Williams, P. D. *Inorg. Chem.* **1983**, *22*, 2661–2662.
(11) Brunner, H.; Kauermann, H.; Meier, W.; Wachter, J. *J. Organomet. Chem.* **1984**, *263*, 183–192.
(12) Brunner, H.; Meier, W.; Wachter, J.; Weber, P.; Ziegler, M. L.; Enemark, J. H.; Young, C. G. *J. Organomet. Chem.* **1986**, *309*, 313–318.
(13) Kubas, G. J.; Ryan, R. R.; Kubatmartin, K. A. *J. Am. Chem. Soc.* **1989**, *111*, 7823–7832.
(14) Birnbaum, J.; Godziela, G.; Maciejewski, M.; Tonker, T. L.; Haltiwanger, R. C.; Rakowski Dubois, M. *Organometallics* **1990**, *9*, 394–401.
(15) Newell, R.; Ohman, C.; Rakowski DuBois, M. *Organometallics* **2005**, *24*, 4406–4415.
(16) Appel, A. M.; DuBois, D. L.; Rakowski DuBois, M. *J. Am. Chem. Soc.* **2005**, *127*, 12717–12726.
(17) Rüchardt, C.; Gerst, M.; Ebenhoch, J. *Angew. Chem., Int. Ed. Engl.* **1997**, *36*, 1406–1430.
(18) Sweany, R. L.; Halpern, J. *J. Am. Chem. Soc.* **1977**, *99*, 8335–8337.
(19) Halpern, J. *Pure Appl. Chem.* **1986**, *58*, 575–584.
(20) Eisenberg, D. C.; Norton, J. R. *Isr. J. Chem.* **1991**, *31*, 55–66.
(21) Gridnev, A. A.; Ittel, S. D. *Chem. Rev.* **2001**, *101*, 3611–3660.
(22) Tang, L.; Norton, J. R. *Macromolecules* **2006**, *39*, 8236–8240.
(23) Tang, L.; Norton, J. R. *Macromolecules* **2006**, *39*, 8229–8235.
(24) Choi, J.; Tang, L.; Norton, J. R. *J. Am. Chem. Soc.* **2007**, *129*, 234–240.

10.1021/ja078115r CCC: $40.75

reactions.[26–28] The formation of persistent radicals,[29–36] either due to slow or readily reversible dimerization, can result in living polymerization or catalytic hydrogenation by reverse-radical-disproportionation (eq 1), depending upon the strength of the

$$MH + R_2C{=}CR'_2 \rightarrow M\bullet + R_2\dot{C}{-}CHR'_2 \qquad (1)$$

bond to hydrogen. Equation 2 illustrates the putative mechanism for stepwise hydrogenolytic cleavage of carbon−carbon bonds facilitated by reactive M−H or S−H bonds of heterogeneous molybdenum sulfide catalysts (represented by $Mo_2S_4H_2$). This is suggested to be a general mechanism for hydrogenation (eq 3) and hydrogenolysis during hydropyrolysis of carbonaceous materials such as biomass and coal.[17]

$$Ar{-}R \xrightarrow{Mo_2S_4H_2} ArH + \bullet R \xrightarrow{Mo_2S_4H\bullet} ArH + HR \qquad (2)$$

$$R_2C{=}CR'_2 \xrightarrow{Mo_2S_4H_2} R_2\dot{C}{-}CHR'_2 \xrightarrow{Mo_2S_4H\bullet} R_2CH{-}CHR'_2 \qquad (3)$$

$$Mo_2S_4 \xrightarrow{H_2} Mo_2S_4H_2 \qquad (4)$$

We have reported studies of the hydrogen atom abstraction rate by benzyl radical from $Cp_2Mo_2S_4H_2$ and the relevance of these kinetic studies to reverse-radical-disproportionation based hydrogenation (eq 3) for Mo_nS_{2n} HDS catalysts and C−C bond hydrogenolysis (eq 2).[37] However, the radical resulting from hydrogen atom abstraction from $Cp_2Mo_2S_4H_2$ can donate a second hydrogen atom or undergo disproportionation to form $Cp_2Mo_2S_4$ and $Cp_2Mo_2S_4H_2$, complicating the kinetics and preventing unequivocal observation of S−S bond formation in self-reaction of $Cp_2Mo_2S_4H\bullet$. To simplify the kinetic studies, one of the μ-SH hydrogen atoms was replaced with a methyl group in order to eliminate disproportionation by hydrogen transfer. Next, self-combination of the radical was impeded by use of the more sterically hindered pentamethylcyclopentadienide (Cp*) rather than the unsubstituted Cp ligand.[38] These two approaches were expected to yield a stable or persistent radical. Both approaches have been used in this work to make

Chart 1. Structural Representations and Abbreviations of $Cp^*_2Mo_2S_4$ Complexes in This Work

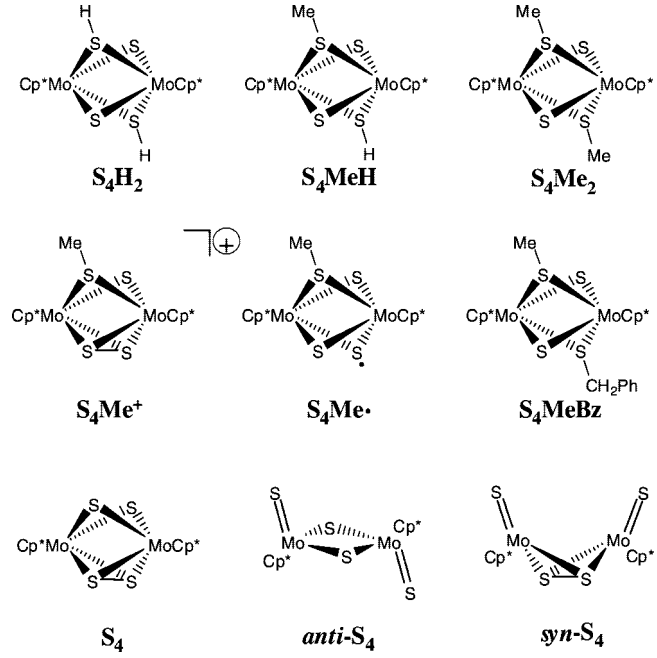

S_4MeH (see Chart 1) and related complexes to investigate the homolysis and formation of S−H and S−S bonds in Mo_2S_4 complexes.

Results and Discussion

Synthesis and Structure of S_4Me^+. S_4H_2 was prepared by the literature methods[7,9] and used for the synthesis of **S_4** by a new route through acid induced H_2 elimination (Scheme 1, reactions a and b). In this approach, reacting **S_4H_2** with an excess of trifluoroacetic acid resulted in formation of **S_4H^+**, which was then deprotonated using triethylamine to give **S_4**. The spectroscopic data of this product matched the previously reported data.[9] However, rather than producing a mixture of **S_4**, ***anti*-S_4**, and ***syn*-S_4**, this method selectively produced **S_4**, which was then used as a starting material for the synthesis of mono and dialkylated **S_4H_2** analogs.

S_4Me^+ was prepared by reaction of methyl triflate with **S_4** (Scheme 1, reaction e) and isolated as the triflate salt rather than the previously reported iodide[11] in order to simplify electrochemical studies. The crystal structure of **S_4Me^+** shows a bridging disulfide with an average sulfur−sulfur distance of 2.06 Å for the two cations observed per asymmetric unit. The disulfide bond is consistent with previously reported structures for **S_4** (2.10 Å)[9] and a similar monoalkylated cationic complex (2.13 Å).[39] The S−CH_3 average distance is 1.81 Å, and the Mo−Mo average distance is 2.63 Å. Figure 1 shows one of the two **S_4Me^+** cations per asymmetric unit in the structure, with selected bond lengths and angles listed in Table 1. Crystallographic data and additional figures with the complete contents of the asymmetric unit are in the Supporting Information.

Synthesis and Reactivity of S_4MeH. S_4MeH was prepared from **S_4** by reaction with methyl lithium followed by protonation of the formed anion (Scheme 1, reactions c and d). The ^{1}H NMR spectrum of this complex was very similar to those of **S_4H_2**

(25) Tsarevsky, N. V.; Matyjaszewski, K. *Chem. Rev.* **2007**, *107*, 2270–2299.
(26) Yet, L. *Tetrahedron* **1999**, *55*, 9349.
(27) Jasperse, C. P.; Curran, D. P.; Fevig, T. L. *Chem. Rev.* **1991**, *91*, 1237–1286.
(28) Smith, D. M.; Pulling, M. E.; Norton, J. R. *J. Am. Chem. Soc.* **2007**, *129*, 770–771.
(29) Daikh, B. E.; Finke, R. G. *J. Am. Chem. Soc.* **1992**, *114*, 2938–2943.
(30) Bravo, A.; Bjorsvik, H. R.; Fontana, F.; Liguori, L.; Minisci, F. *J. Org. Chem.* **1997**, *62*, 3849–3857.
(31) Fischer, H. *Macromolecules* **1997**, *30*, 5666–5672.
(32) Kothe, T.; Marque, S.; Martschke, R.; Popov, M.; Fischer, H. *J. Chem. Soc., Perkin Trans. 2* **1998**, 1553–1559.
(33) Griller, D.; Ingold, K. U. *Acc. Chem. Res.* **1976**, *9*, 13–19.
(34) Fischer, H. *J. Am. Chem. Soc.* **1986**, *108*, 3925–3927.
(35) Fischer, H. *Chem. Rev.* **2001**, *101*, 3581–3610.
(36) Focsaneanu, K. S.; Scaiano, J. C. *Helv. Chim. Acta* **2006**, *89*, 2473–2482.
(37) Franz, J. A.; Birnbaum, J. C.; Kolwaite, D. S.; Linehan, J. C.; Camaioni, D. M.; Dupuis, M. *J. Am. Chem. Soc.* **2004**, *126*, 6680–6691.
(38) Watkins, W. C.; Jaeger, T.; Kidd, C. E.; Fortier, S.; Baird, M. C.; Kiss, G.; Roper, G. C.; Hoff, C. D. *J. Am. Chem. Soc.* **1992**, *114*, 907–914.
(39) Lopez, L. L.; Gabay, J.; Haltiwanger, R. C.; Green, K.; Allshouse, J.; Casewit, C.; Rakowski Dubois, M. *Organometallics* **1993**, *12*, 4764–4770.

Scheme 1. Synthetic Routes to **S_4**, **S_4MeH**, **S_4Me^+**, and **S_4MeBz** by Reactions a through f

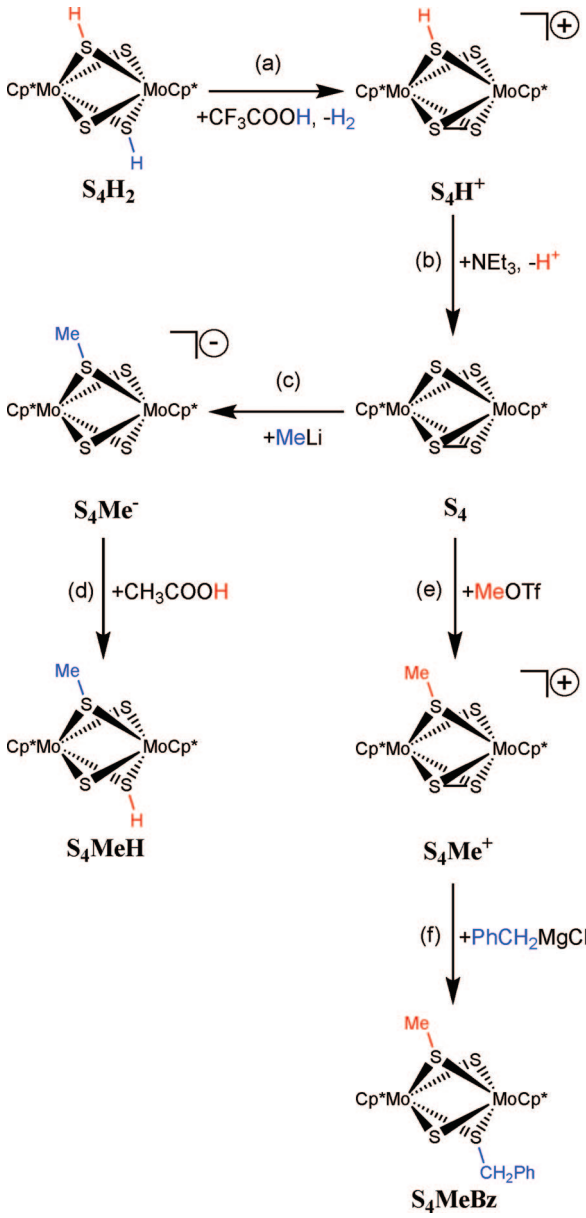

and **S_4Me_2**, including the presence of two different observable isomers (see Chart 2).[7,12] The two isomers are observed in an approximately 2:1 ratio and are assigned as isomers A and B, as they have been computationally shown to be the lowest in energy for $Cp_2Mo_2S_4H_2$.[37] The spectrum contained the Cp* resonance at 2.20 ppm (in CD_3CN), the methanethiolate resonances at 1.07 and 0.99 ppm (isomers B and A, respectively), and the hydrosulfide resonances at −2.33 and −2.51 ppm (isomers B and A, respectively).

S_4MeH was used for kinetic studies of the S−H hydrogen atom abstraction rate of benzyl radical through photolysis of dibenzyl ketone (DBK) in the presence of **S_4MeH** (Scheme 2, reaction a), as previously described for $Cp_2Mo_2S_4H_2$.[37] Figure 2 shows the Eyring plot of the resulting data, and Table 2 contains the rate parameters along with those for $Cp_2Mo_2S_4H_2$ for comparison.

After determining the rate of hydrogen atom abstraction by benzyl radical, additional photolysis experiments were run at a higher concentration of **S_4MeH** in order to directly observe by

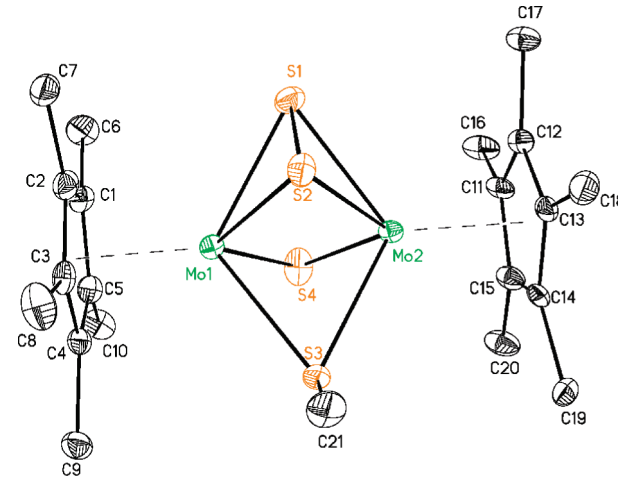

Figure 1. Structure of **S_4Me^+** with 30% thermal displacement. Only one of the two unique **S_4Me^+** cations is shown, and hydrogen atoms, counterions, and solvent molecules are omitted for clarity.

Table 1. Selected Bond Distances and Angles for One of the Two Unique **S_4Me^+** Cations per Asymmetric Unit

distances, Å		angles, deg	
Mo(1)−Mo(2)	2.6311(7)	C(21)−S(3)−Mo(1)	111.9(2)
S(1)−S(2)	2.050(2)	C(21)−S(3)−Mo(2)	112.2(2)
S(2)···S(3)	3.145	Mo(1)−S(1)−Mo(2)	65.62(4)
S(3)···S(4)	2.910	Mo(1)−S(2)−Mo(2)	65.31(4)
S(4)···S(1)	3.136	Mo(2)−S(3)−Mo(1)	64.75(4)
C(21)−S(3)	1.820(6)	Mo(2)−S(4)−Mo(1)	69.89(5)
Mo(1)−S(1)	2.4255(16)	S(1)−Mo(1)−S(2)	49.95(6)
Mo(1)−S(2)	2.4310(15)	S(1)−Mo(2)−S(2)	49.74(6)
Mo(1)−S(3)	2.4627(15)	S(1)−S(2)−Mo(1)	64.89(6)
Mo(1)−S(4)	2.2984(17)	S(1)−S(2)−Mo(2)	64.74(6)
Mo(2)−S(1)	2.4300(16)	S(2)−Mo(1)−Mo(2)	57.61(4)
Mo(2)−S(2)	2.4452(15)	S(2)−Mo(2)−Mo(1)	57.09(4)
Mo(2)−S(3)	2.4512(15)	S(2)−S(1)−Mo(1)	65.17(6)
Mo(2)−S(4)	2.2953(16)	S(2)−S(1)−Mo(2)	65.52(6)
Mo−C (average)	2.325		

Chart 2. Structural Representations for the Isomers of the Sulfur Core in $Cp_2Mo_2S_4R_2$ Complexes, As Viewed Down the Mo−Mo Axis

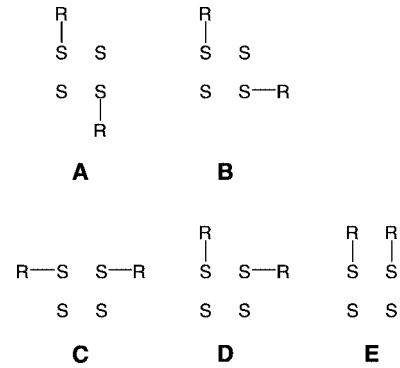

^{1}H NMR the products resulting from cross-termination of **$S_4Me•$** radical with benzyl radical and self-termination of **$S_4Me•$** to form a dimer. In these experiments, the primary radical termination product observed for the resulting **S4Me•** was the cross-termination product, **S_4MeBz**, suggesting slow or reversible dimerization, consistent with the persistent radical effect.[29–36] The cross-termination reaction is shown in Scheme 2, reaction c, and Scheme 3, eq 9. The depletion of **S_4MeH** and the growth of **S_4MeBz** as a function of photolysis time can be observed from the methanethiolate, benzylthiolate (methylene), and

Table 2. Rate Parameters for the Reaction of Benzyl Radical with μ-SH in **S_4MeH** and Previously Reported Kinetic Results for Comparison[a]

hydrogen donor	k (M^{-1} s^{-1}) 298 K	T range (K)	mean temp (T_m, K)	$\Delta S^{\ddagger}$ (eu) (T_m, K)	log A^c (M^{-1} s^{-1})	$\Delta H^{\ddagger}$ (kcal/mol)	$E_a{}^c$ (kcal/mol)
S_4MeH	1.3×10^6	295−353	325	-25.5 ± 0.8	7.68 ± 0.17	1.54 ± 0.25	2.13 ± 0.25
$Cp_2Mo_2S_4H_2$[b]	2.6×10^6	295−372	331	-19.2 ± 1.8	9.07 ± 0.38	2.96 ± 0.58	3.62 ± 0.58
2-naphthalenethiol[b]	1.3×10^5	298−376	337	-23.2 ± 0.8	8.21 ± 0.17	3.57 ± 0.26	4.24 ± 0.26
1-octanethiol[b]	3.1×10^4	295−374	341	-24.7 ± 1.6	7.89 ± 0.35	3.96 ± 0.54	4.64 ± 0.54

[a] All measurements were made in benzene, errors are 2σ. [b] Franz, J. A.; Birnbaum, J. C.; Kolwaite, D. S.; Linehan, J. C.; Camaioni, D. M.; Dupuis, M. *J. Am. Chem. Soc.* **2004,** *126*, 6680−6691. [c] A = Arrhenius pre-exponential factor, E_a = Arrhenius expression, $k = Ae^{-E_a/RT}$.

Scheme 2. Formation and Reactions of **S_4Me•**

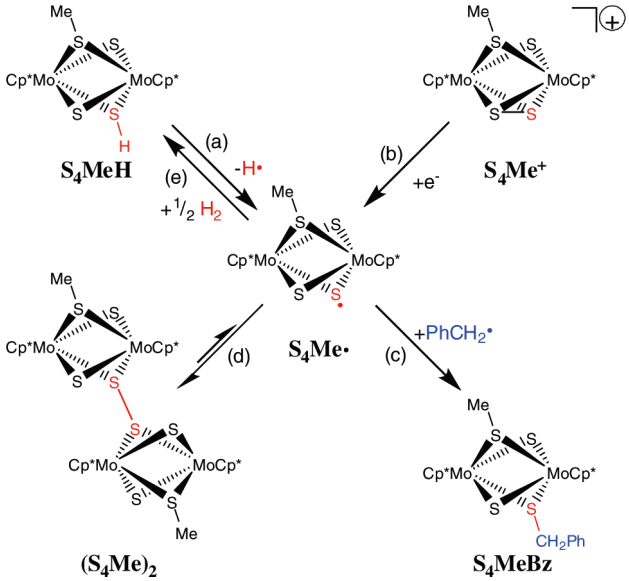

hydrosulfide NMR signals (Figure 3). Two isomers are observed for each complex, giving two methyl and hydrosulfide resonances for **S_4MeH** and two methylene and methyl resonances for **S_4MeBz** (see Chart 2, above).

In order to verify the primary termination product, **S_4MeBz** was synthesized by the reaction of **S_4Me^+** with benzylmagnesium chloride (Scheme 1, Reaction f) and compared by ^{1}H NMR, giving matching synthetic and photolytic products with the exception of the A:B isomeric ratios, which were approximately 10:1 for the synthetic product and 1:2 for the photolytic product. However, after several days in solution the isomeric ratio for A:B reached 3:2, which is the same ratio reported for $Cp_2Mo_2S_4H_2$.[7] The Cp* and methanethiolate resonances of **S_4MeBz** were very similar to those of **S_4MeH**,

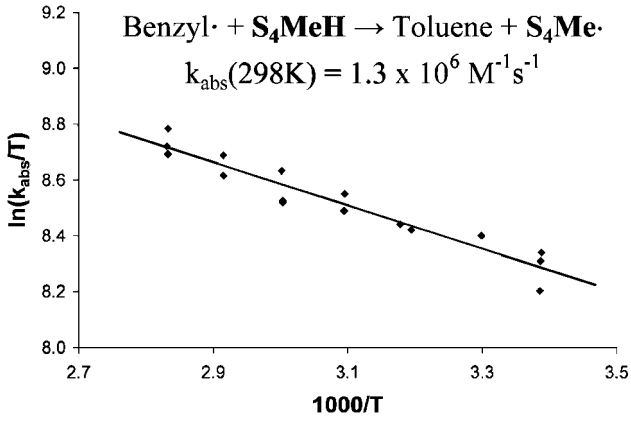

Figure 2. Temperature-dependent rate data for abstraction of hydrogen atom by benzyl radical from **S_4MeH** in benzene.

Scheme 3. Primary Reactions in Steady-State Kinetics of Reaction of Benzyl Radical and S_4MeH

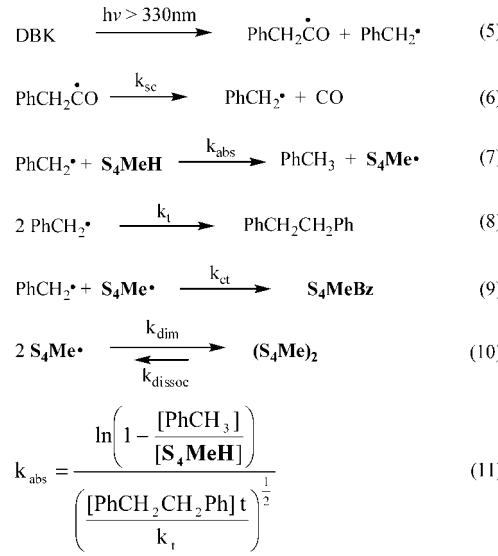

but exhibit the additional methylene and aromatic resonances from the benzyl group and the loss of the hydrosulfide resonances. The aromatic resonances were observed at 7.08, 7.03, and 6.94 ppm, the methylene resonances at 2.82 and 2.78 ppm (assigned as isomers B and A, respectively), Cp* resonances were observed at 2.16 and 2.14 ppm (isomers A and B), and the methanethiolate resonances at 1.14 and 1.00 ppm (isomers B and A). To confirm this formulation, crystals of the synthetically prepared **S_4MeBz** were grown by slow evaporation from a benzene solution, and the structure is shown in Figure 4 with selected bond lengths and angles given in Table 3.

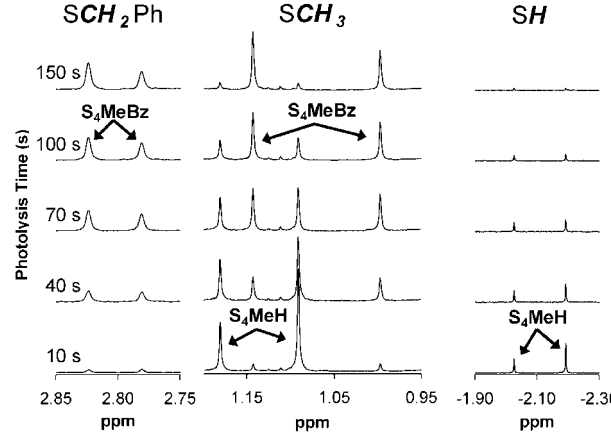

Figure 3. ^{1}H NMR spectra of the photolysis of DBK and **S_4MeH**, showing the depletion of **S_4MeH** and formation of **S_4MeBz** from the methylene (left), methyl (center), and hydrosulfide (right) regions as a function of photolysis time. Two isomers are observed for each complex (see Chart 2). The sample was photolyzed in C_6D_6 at room temperature up to 150 s total photolysis time.

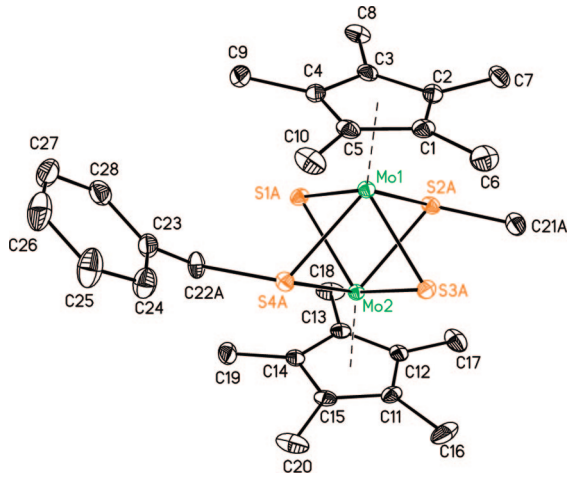

Figure 4. Structure of **S$_4$MeBz** with 30% thermal displacement. Only the primary position for the bridging sulfide and thiolate ligands is shown for one of the two unique **S$_4$MeBz** moieties in the asymmetric unit. Hydrogen atoms, counterions, and solvent molecules are omitted for clarity.

Table 3. Selected Bond Distances and Angles for One of the Two Unique **S$_4$MeBz** Moieties per Asymmetric Unit

distances, Å		angles, deg	
Mo(1)−Mo(2)	2.5758(5)	Mo(1)−S(1A)−Mo(2)	65.75(3)
S(2A)−C(21A)	1.835(15)	Mo(1)−S(3A)−Mo(2)	66.74(3)
S(4A)−C(22A)	1.860(4)	Mo(2)−S(2A)−Mo(1)	62.44(2)
Mo(1)−S(1A)	2.3719(10)	Mo(2)−S(4A)−Mo(1)	62.47(2)
Mo(1)−S(2A)	2.4891(10)	C(21A)−S(2A)−Mo(1)	113.0(6)
Mo(1)−S(3A)	2.3376(10)	C(21A)−S(2A)−Mo(2)	113.6(2)
Mo(1)−S(4A)	2.4877(10)	C(22A)−S(4A)−Mo(1)	116.22(17)
Mo(2)−S(1A)	2.3745(10)	C(22A)−S(4A)−Mo(2)	112.00(13)
Mo(2)−S(2A)	2.4818(10)	C(23)−C(22A)−S(4A)	111.9(3)
Mo(2)−S(3A)	2.3466(10)		
Mo(2)−S(4A)	2.4806(10)		
Mo−C (average)	2.343		

The asymmetric unit contains two **S$_4$MeBz** and two benzene molecules, and the bridging sulfide and alkylthiolate ligands in each **S$_4$MeBz** unit are disordered into two positions with occupancies of 89% and 11%. The average distances are 2.58 Å for Mo−Mo, 1.84 Å for S-CH_3, and 1.85 Å for S-CH_2Ph. The average Mo−S distances are 2.36 Å, 2.49 Å, and 2.48 Å for the sulfides, methanethiolates, and benzylthiolates, respectively. The crystal structure contains only isomer A (see Chart 2), which is expected to correspond to the primary isomer observed in the NMR spectra for the synthetic product. Although the second isomer observed in the NMR spectrum is not observed in the crystal structure, it is predicted to be isomer B, based on the previously calculated isomers for $Cp_2Mo_2S_4H_2$.[37]

In addition to isomers A and B, a third product was observed in the photolysis experiments, and this product may be one of the cis isomers of **S$_4$MeBz** (Scheme 4, Reaction c). While the cis isomers are usually not observed for the S_4R_2 complexes, benzyl addition by a radical pathway may result in the formation of different isomers than are observed by other synthetic routes. The observed isomer is expected to be isomer C or D in Chart 2, as the relative energies of these isomers for $Cp_2Mo_2S_4H_2$ have been previously calculated to be similar, whereas isomer E is expected to be significantly higher in energy.[37]

Investigation of this third product, which exhibited a Cp* methyl resonance at 1.90 ppm, revealed that it slowly converts to ***trans*-S$_4$MeBz** isomers A and B (approximately 75% conversion was observed in one week). The slow conversion to isomers

Scheme 4. Transient Intermediate, Suggested To be ***cis*-S$_4$MeBz**, Is Observed Both in the Reaction (a) of Benzyl Radical with S_4MeH and in the Photoreaction (g) of ***trans*-S$_4$MeBz** with Benzyl Radical[a]

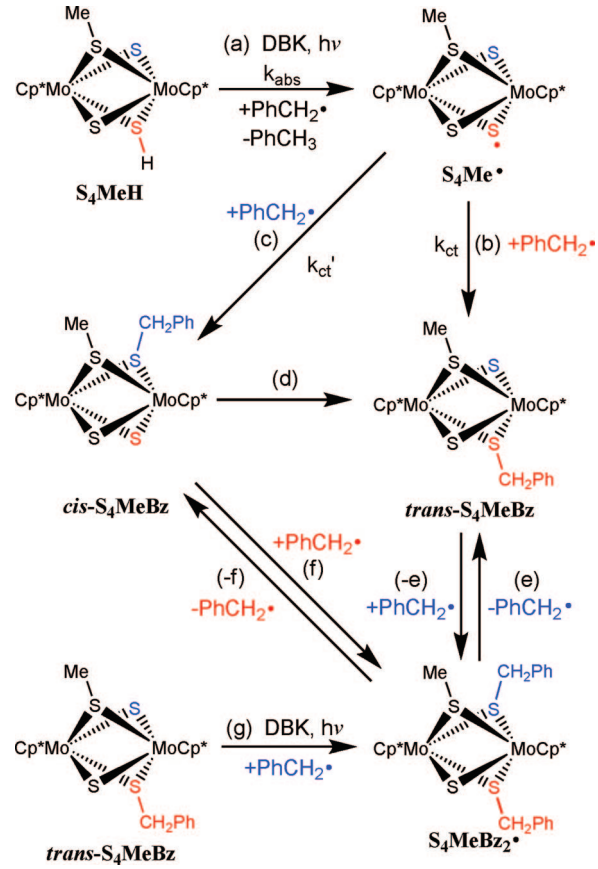

[a] In both cases, ***cis*-S$_4$MeBz** undergoes slow thermal isomerization (d) to ***trans*-S$_4$MeBz**. Pathway (d) may occur via addition/scission pathways (e,f).

A and B suggests that the product is very likely one of the less stable *cis* cross-termination product isomers. Further evidence for the intermediacy of ***cis*-S$_4$MeBz** was developed by photolysis of a solution of the two isomers of ***trans*-S$_4$MeBz** in benzene (Scheme 4, Reaction g). Without added DBK, no photoreaction was observed. However, with added DBK, the identical intermediate, proposed to be one of the possible isomers of ***cis*-S$_4$MeBz**, was formed and was observed to convert in a dark reaction to the two isomers of ***trans*-S$_4$MeBz**. Thus, addition of benzyl radical to ***trans*-S$_4$MeBz** and scission to give both isomers (Scheme 4, pathways e,f) appears facile, possibly by a slow chain reaction involving addition/scission of benzyl radical to the Mo_2S_4 core.

Reduction of S$_4$Me$^+$. By cyclic voltammetry, two reversible waves are observed for the reduction of **S$_4$Me$^+$** in acetonitrile, with half-wave potentials of −0.93 and −1.30 V vs ferrocene and peak separations of 59 and 62 mV at 0.5 V/s. These data suggest that a stable product could be isolated from a one-electron reduction of the cation at a potential between the two waves, with the overall reaction shown in Scheme 2, reaction b. **S$_4$Me$^+$** was reduced in acetonitrile both by controlled potential electrolysis, passing 3.9 C (4.3 C expected for one electron reduction), and by chemical reduction using 1 equiv. of bis(benzene) chromium(0)[40] to give a purple precipitate with

(40) Connelly, N. G.; Geiger, W. E. *Chem. Rev.* **1996**, *96*, 877–910.

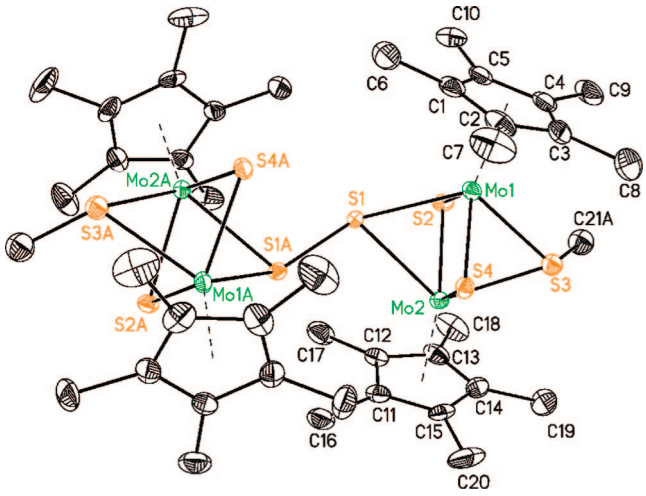

Figure 5. Structure of $(\mathbf{S_4Me})_2$ with 30% thermal displacement, where the two $\mathbf{S_4Me}$• units are symmetry related (2-fold axis). Only one of the disordered sulfide and methanethiolate positions is shown, and the hydrogen atoms and solvent molecules are omitted for clarity.

Table 4. Selected Bond Distances and Angles for $(\mathbf{S_4Me})_2$

distances, Å		angles, deg	
Mo(1)−Mo(2)	2.5940(5)	C(21A)−S(3)−Mo(1)	116.4(4)
S(1)−S(1A)	2.059(3)	C(21A−S(3)−Mo(2)	115.3(4)
S(3)−C(21A)	1.782(8)	Mo(1)−S(1)−Mo(2)	62.37(4)
Mo(1)−S(1)	2.4760(16)	Mo(1)−S(2)−Mo(2)	66.15(5)
Mo(1)−S(2)	2.3537(18)	Mo(1)−S(3)−Mo(2)	63.67(5)
Mo(1)−S(3)	2.454(2)	Mo(1)−S(4)−Mo(2)	67.71(5)
Mo(1)−S(4)	2.2966(17)	S(1A)−S(1)−Mo(1)	141.03(6)
Mo(2)−S(1)	2.5326(17)	S(1A)−S(1)−Mo(2)	106.82(10)
Mo(2)−S(2)	2.3994(17)		
Mo(2)−S(3)	2.464(2)		
Mo(2)−S(4)	2.3592(18)		
Mo−C (average)	2.353		

matching spectroscopic data from either method. Additionally, cyclic voltammetry in THF resulted in equivalent data from $\mathbf{S_4Me}^+$ and the products of the reductions. Recrystallization of this solid by vapor diffusion of acetonitrile into a toluene solution of the product gave crystals suitable for analysis by X-ray diffraction. The crystal structure revealed a dimer of two $\mathbf{S_4Me}$• units, making a tetranuclear complex with a bridging disulfide bond between the Mo_2S_4 cores. The structure of the dimer is shown in Figure 5, with selected bond lengths and angles in Table 4.

The two $\mathbf{S_4Me}$• units in the dimer are symmetry related (2-fold axis) and have a Mo(1)−Mo(2) distance of 2.59 Å. The methanethiolate on each monomer is disordered into three positions, giving an average S−CH_3 bond length of 1.79 Å. Isomers A and B (Chart 2) can be assigned using the relative orientations of the bridging disulfide bond and the S−C bond of the methanethiolate in one $\mathbf{S_4Me}$• unit, where two of the disordered methanethiolate positions correspond to isomer A (75% occupancy), and the remaining position corresponds to isomer B (25% occupancy). The disulfide (S(1)) and two bridging sulfide ligands (S(2) and S(4)) in each monomer are disordered into two different sets of positions. The average bond length for the disulfide bridging the two $\mathbf{S_4Me}$• units is 2.14 Å, which is consistent with previously reported bridging disulfide bond lengths in analogous dimers,[14] as well as other internal disulfide bonds (see $\mathbf{S_4Me}^+$, above). While steric strain for dimer formation is not evident from the length of the bridging disulfide bond, the Cp* rings at each end of the Mo_2S_4 units are

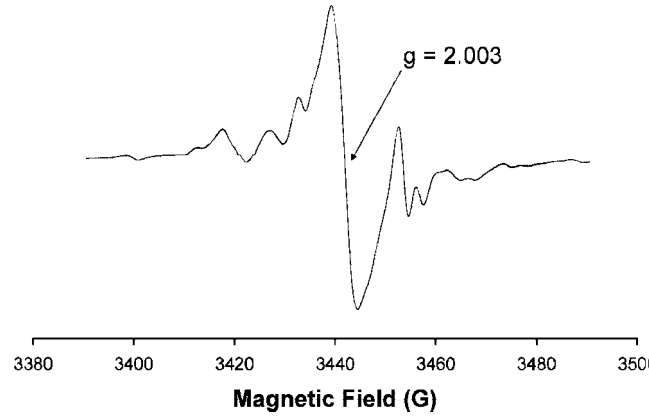

Figure 6. EPR spectrum of 5 mM $(\mathbf{S_4Me})_2$ in toluene at 23 °C with g = 2.003.

Chart 3. Structural Representations for the Possible Isomers of the Sulfur Core in the $\mathbf{S_4Me}$• Radical, As Viewed Down the Mo−Mo Axis

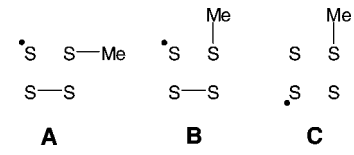

significantly tilted away from the neighboring $\mathbf{S_4Me}$•, forming a dihedral angle of 12.7° between the C(1)−C(10) and C(11)−C(20) planes. This tilting of the rings illustrates the steric crowding occurring between the Cp* rings on the two $\mathbf{S_4Me}$• units, and has further implications for the low temperature NMR data, as discussed below. Additional crystallographic figures and data are given in the Supporting Information.

Magnetic Studies of $(\mathbf{S_4Me})_2$. A solution of $(\mathbf{S_4Me})_2$ in toluene was used to collect the EPR spectrum shown in Figure 6. While the dimer itself is expected to be diamagnetic, dissociation into $\mathbf{S_4Me}$• would give a paramagnetic complex, giving an EPR spectrum similar to those reported for $(CpMo)_2(\mu\text{-}S)(\mu\text{-}SCH_3)S_2CH_2$ and $[MeCpMo(\mu\text{-}S)(\mu\text{-}SCH_3)]_2K$, including the hyperfine coupling to $I = {}^5/_2$ molybdenum nuclei.[41,42] In the case of the $\mathbf{S_4Me}$• radical, the EPR spectrum is expected to be more complex than those previously reported. The spectrum may be a composite spectrum of as many as three possible isomeric forms of the radical, as illustrated in Chart 3. Isomers A and B are analogous to the isomers discussed above for $\mathbf{S_4R_2}$ complexes, except with a disulfide bond as the point of reference rather than a bond to a second substituent. A and B are expected to be close in energy, reminiscent of the two predominant isomers of $Cp_2Mo_2S_4H_2$.[7,37] Isomer C, however, is a distinct structure, lacking the disulfide bond. Computational studies reveal isomer C to be 6 kcal/mol less stable than A, suggesting that isomer C does not contribute significantly to the EPR spectrum, as it will be inadequately populated to be observable.[43] On the basis of these computational results, the observed EPR spectrum is expected to result from a combination of isomers A and B. The Supporting Information contains further details of the EPR spectrum and simulations of this complex spectrum using two isomers. Further evidence that the complex EPR

(41) Casewit, C. J.; Haltiwanger, R. C.; Noordik, J.; Rakowski Dubois, M. *Organometallics* **1985**, *4*, 119–129.
(42) Casewit, C. J.; Rakowski Dubois, M. *Inorg. Chem.* **1986**, *25*, 74–80.
(43) UB3LYP electronic structure calculations reveal C to be 6 kcal/mole less stable than A. Results to be published separately.

spectrum resulted from **S_4Me•** and not an unrelated impurity is shown in the collection of EPR spectra at multiple concentrations and the reaction of the sample with hydrogen, both discussed below.

The solid state dimer structure and the solution EPR spectra suggest the interconversion of **$(S_4Me)_2$** and **S_4Me•** (Scheme 2, reaction d). In order to determine the extent of dimer formation in solution (eq 12), the Evans method was used to measure the magnetic susceptibility by ^{1}H NMR.[44,45] In this method, a sealed capillary tube containing a pure solvent is placed in an NMR tube containing a solution of the analyte in the same solvent. The difference in chemical shift between the pure solvent and the solvent containing analyte is proportional to the magnetic susceptibility of the analyte.

$$K_{\mathrm{dim}} = \frac{[(S_4Me)_2]}{[S_4Me]^2} \qquad (12)$$

However, a 0.018 M solution of **$(S_4Me)_2$** in toluene resulted in a single peak for the toluene methyl group, indicating a low level of paramagnetism. The lower limit for the equilibrium constant for dimer formation (K_{dim}) can be estimated from the NMR spectrum given that the difference in chemical shift between the pure solvent peak and the solvent peak for the analyte solution is less than the observed line width, 3 Hz. Assuming that the radical **S_4Me•** would have one unpaired electron with a spin-only μ_{eff} of 1.73, as would be expected given the g value of 2.003 observed in the EPR spectrum, the maximum concentration of radical in this solution is 8.1×10^{-4} M, giving $K_{\mathrm{dim}} > 2.7 \times 10^4$ M^{-1}.

In order to better quantify the radical-dimer equilibrium, the EPR spectrum of solutions of **$(S_4Me)_2$** were collected at 16, 4.1, and 1.1 mM concentrations, and spectra of TEMPO at 8.4×10^{-5} M were collected under identical conditions. The spectra of both TEMPO and **$(S_4Me)_2$** were then double integrated to determine the concentration of **S_4Me•**, resulting in an average equilibrium constant of $5.7 \times 10^4 \pm 2.1 \times 10^4$ M^{-1} from 9 experiments. This equilibrium constant corresponds to a dimer bond dissociation free energy of 6.5 kcal/mol at 25 °C. The determined equilibrium constant is in line with the limit provided by the magnetic susceptibility experiments and is just outside of the range observable in that experiment. While the line shape for the EPR spectra does not change with concentration, the total intensity does. Figure 7 shows the experimental EPR spectra after correcting for the expected change in radical concentration based upon the change in initial dimer concentration, as described by Eq 12. Specifically, decreasing the total **$(S_4Me)_2$** concentration by a factor of 4 results in a factor of 2 decrease in **S_4Me•** concentration.

Variable Temperature NMR Spectroscopy of $(S_4Me)_2$. At temperatures of +10 °C or higher, a broad singlet was observed for the Cp* resonance in the ^{1}H NMR of **$(S_4Me)_2$** in toluene-d_8. This peak shifted downfield with increasing temperature or decreasing concentration, a consequence of the increase in the radical to dimer ratio resulting from the greater extent of dissociation at higher temperatures or in more dilute solutions.[46] At temperatures above 50 °C, substantial decomposition occurred within 15 min, resulting in the formation of equal amounts of **S_4Me_2** and ***anti*-S_4**, as well as additional unidentified

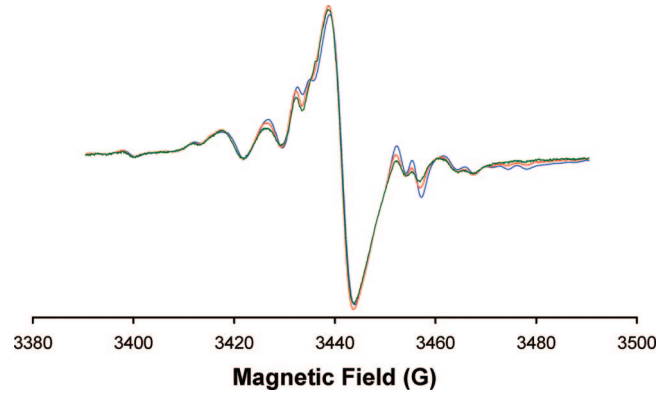

Figure 7. Experimental EPR spectra for 16 mM (blue), 4.1 mM (red), and 1.1 mM (green) solutions of **$(S_4Me)_2$** after correcting for the concentration dependence of the radical-dimer equilibrium. The spectra were collected in toluene at 23 °C.

products. The formation of **S_4Me_2** and ***anti*-S_4** suggests that a primary decomposition pathway for **S_4Me•** is disproportionation by methyl transfer, much like the reported transfer for $(MeCpMo)_2(S)(SCH_3)(S_2CH_2)$ at reflux in THF to give $(MeCpMoS_2)_2(S_2CH_2)$ and $(MeCpMo(SCH_3)_2)_2(S_2CH_2)$.[47] If **$(S_4Me)_2$** disproportionates by methyl transfer, then **S_4Me_2** and **S_4** would be the expected products; however, it would be predicted that **S_4** would undergo facile isomerization to ***anti*-S_4** given that **S_4** can be thermally[9] and photochemically[48] converted to ***syn*-S_4** and ***anti*-S_4**, and that computationally, the anti isomer has been determined to be the most stable isomer of $Cp_2Mo_2S_4$.[37]

Below 10 °C, the broad Cp* resonance in the ^{1}H NMR spectrum stopped shifting and began to resolve. Similarly, methanethiolate peaks were not discernible at room temperature but were observed below −1 °C, showing two primary isomers in a 1.7:1 ratio, similar in both chemical shift and relative ratio to those observed for **S_4MeH**. At −1 °C, the Cp* resonance resolved into two broad peaks. Upon further cooling to −33 °C, each of these two peaks resolved into four singlets, with one of the singlets having twice the area of the others (relative areas of 3:3:3:6). From the crystal structure of **$(S_4Me)_2$**, it can be seen that the bridging disulfide is asymmetric relative to the two Cp* rings on each unit, as illustrated in Figure 8, resulting in two different chemical environments for the Cp* rings, consistent with the NMR data at −1 °C. Furthermore, both the observed close proximities of the Cp* methyl groups in the crystal structure and the inequivalency of the methyl groups on each Cp* that is observed in the NMR spectra at −33 °C suggest that the Cp* methyl groups are sufficiently crowded to hinder ring rotation and thereby rapid site exchange of the methyl groups while in the **$(S_4Me)_2$** form.

The use of low temperature NMR data has been previously reported for the determination of the dissociation rate constants for $[Cp^*Cr(CO)_3]_2$ and $[CpCr(CO)_3]_2$.[46] For these species, the rate constants for dissociation were reported to be proportional to the line width for the average Cp or Cp* resonances over the temperature range in which the resonances were not paramagnetically shifted or broadened. In the case of **$(S_4Me)_2$**, the low temperature NMR spectra reveal the expected inequivalence of the Cp* methyl resonances. In order to determine the rate constants for exchange from the ^{1}H NMR spectra, the

(44) Evans, D. F. *J. Chem. Soc.* **1959**, 2003–2005.
(45) Sur, S. K. *J. Magn. Reson.* **1989**, *82*, 169–173.
(46) Woska, D. C.; Ni, Y. P.; Wayland, B. B. *Inorg. Chem.* **1999**, *38*, 4135–4138.
(47) Casewit, C. J.; Rakowski Dubois, M. *J. Am. Chem. Soc.* **1986**, *108*, 5482–5489.
(48) Bruce, A. E.; Tyler, D. R. *Inorg. Chem.* **1984**, *23*, 3433–3434.

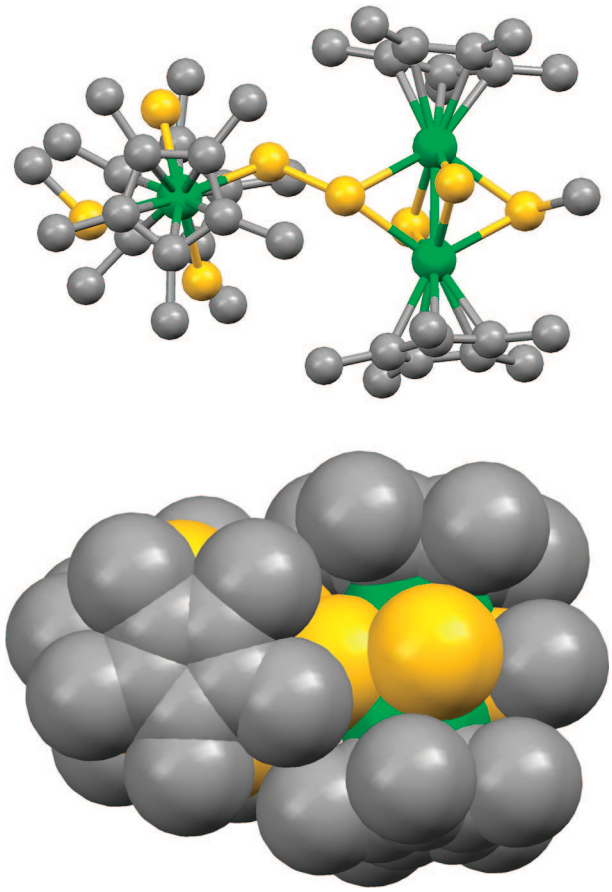

Figure 8. Ball and stick and space-filling models of **$(S_4Me)_2$** using crystallographic data, illustrating Cp* inequivalence due to the bridging disulfide (top) and the steric constraint around each Cp* (bottom), both consistent with the variable temperature NMR data. Hydrogen atoms have been omitted for clarity.

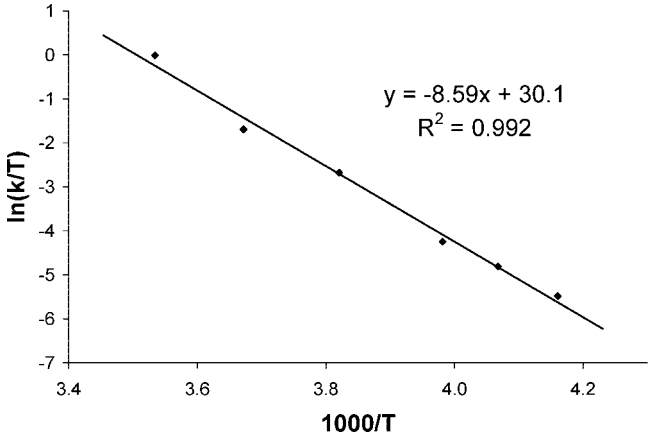

Figure 9. Eyring plot of site exchange rate from **$(S_4Me)_2$** low temperature NMR data, giving $\Delta H^{\ddagger}$ of 17.1 ± 1.5 kcal/mol and $\Delta S^{\ddagger}$ of 12.6 ± 6.0 cal/mol K.

methanethiolate and Cp* methyl resonances were simulated from +10 to −33 °C using SpinWorks[49] (details of the simulations are included in the Supporting Information). An Eyring plot of these data is shown in Figure 9 and results in $\Delta H^{\ddagger}$ of 17.1 ± 1.5 kcal/mol and $\Delta S^{\ddagger}$ of 12.6 ± 6.0 cal/mol K. The Eyring plot contains data for both the Cp* methyl group exchange and the methanethiolate exchange and results in a linear plot, suggesting that both exchange processes occur by the same mechanism, dimer dissociation and redimerization. This is further supported by the fact that rapid interconversion of the methanethiolate isomers by inversion at the sulfur centers is not observed for $Cp^*_2Mo_2S_4R_2$ complexes, as is evident in the reported chromatographic separation for the isomers of **S_4Me_2** and the lack of exchange for the isomeric hydrosulfido resonances of $Cp_2Mo_2S_4H_2$ up to 90 °C.[7,12] The normally slow inversion of sulfur centers suggests that a different mechanism is the source of the methanethiolate exchange in this system.

Dimer dissociation and the following redimerization would result in exchange of both the methanethiolate resonances and the Cp* methyl groups, and this process is already known to occur as a result of the observed equilibrium from the magnetic susceptibility and EPR data, and the matching cyclic voltammetry data for **S_4Me^+** and **$(S_4Me)_2$** in THF. If **$S_4Me•$** and **$(S_4Me)_2$** did not interconvert rapidly at room temperature, then the cyclic voltammograms for **S_4Me^+** and **$(S_4Me)_2$** would not be expected to match. Given the equilibrium constant of 5.7×10^4 M^{-1} for K_{dim} from the EPR data, the dimer is the predominant form at millimolar concentrations at room temperature, indicating that the dimerization rate constant is larger than the dissociation rate constant. Consequently, dissociation appears to be the rate-limiting step in the exchange process, consistent with the observed concentration independent low temperature NMR data. Using the kinetic parameters from the Eyring plot for the exchange process, given that these parameters appear to be for the dissociation of **$(S_4Me)_2$**, the rate constant for dissociation can be calculated to be 1.1×10^3 s^{-1} at 25 °C.

Using the rate constant for the dissociation of the dimer and the equilibrium constant for dimerization (1.1×10^3 s^{-1} and 5.7×10^4 M^{-1} at 25 °C), the rate constant for dimerization can be calculated to be 6.3×10^7 M^{-1} s^{-1} at 25 °C in toluene. In the photolysis experiments, the exclusive formation of cross-termination products and the lack of formation of the self-termination product **$(S_4Me)_2$** is consistent with the Fischer−Ingold persistent radical effect,[29–36] and in this case, may be the result of both reversible dimerization and appreciably reduced self-termination rates.

Reaction of $(S_4Me)_2$ with Hydrogen. Previously reported disulfide bridged dimers have been reduced in a hydrogen atmosphere to give the monomeric S−H complexes.[14] In the analogous reaction, a solution of **$(S_4Me)_2$** in toluene-d_8 was purged with hydrogen to test for conversion to **S_4MeH** (Scheme 2, reaction e). The reaction occurred readily at room temperature, with nearly 60% completion after 10 min total reaction time and quantitative conversion of **$(S_4Me)_2$** to **S_4MeH** in 30 min. In a similar experiment, an EPR spectrum of a solution of **$(S_4Me)_2$** in toluene was collected, and then the sample was purged with hydrogen and the EPR spectrum again collected, resulting in the EPR signal being reduced to the baseline. Both of these experiments show that the **$(S_4Me)_2$/$S_4Me•$** mixture can be converted to the diamagnetic **S_4MeH** by reaction with hydrogen, and that both the NMR and EPR signals are consistent with the assignments to **$(S_4Me)_2$** and **$S_4Me•$**.

The reaction of **$(S_4Me)_2$** with hydrogen offers a clean, simple route for the synthesis of **S_4MeH** from **S_4Me^+** by chemical reduction and hydrogenation and does not require the chromatographic separation of **S_4MeH** from **S_4Me_2** and **S_4H_2** that is needed after methylation and protonation of **S_4**. The conversion of **$(S_4Me)_2$** to **S_4MeH** under 1 atm of hydrogen at room temperature also demonstrates that the effective S−H homolytic

(49) Marat, K. *SpinWorks*, v. 2.5.5; 2005.

bond dissociation free energy for **S_4MeH** to the dimer/radical mixture is greater than 52 kcal/mol, as the reaction goes to completion (the sum of two S−H bond dissociation free energies is greater than the homolytic bond dissociation free energy of H_2, which is approximately 104 kcal/mol).[50] Given that gas phase homolytic bond dissociation enthalpies are expected to be 5 kcal/mol higher than solution bond dissociation free energies,[50] the S−H bond enthalpy is estimated to be greater than 57 kcal/mol. Complete thermochemical studies of the homolytic and heterolytic S−H bond dissociation free energies of **S_4H_2** and **S_4MeH** are currently in progress. These studies will provide additional insight into the reactivities of the S−H bonds in Mo_2S_4 clusters.

Conclusions

A variety of reactions have been demonstrated at the sulfur centers in Mo_2S_4-based homogeneous analogs of HDS catalysts, including hydrogen atom transfer, hydrogen addition, alkyl group addition and transfer, and disulfide formation and cleavage. All of these reactions are key steps in HDS catalysis and are important for wide range of chemistry. For Mo_2S_4 complexes, the formation and cleavage of disulfide bonds help to control the reactivity and form stable complexes. The observed disulfide bridged tetranuclear complex, **$(S_4Me)_2$**, shows a very weak disulfide bond dissociation free energy of 6.5 kcal/mol. This weak disulfide bond formation results in a radical-dimer equilibrium and gives rise to selective reactivity with carbon centered radicals, typical of persistent free radicals. While increasing the steric bulk of the complex and substituting a methyl group for one of the hydrogen atoms did not completely prevent dimerization, disproportionation is substantially slower, although not eliminated. Understanding the kinetics and thermodynamics for the formation and cleavage of bonds to hydrogen are key to understanding and developing many catalytic and chemical processes, and the reactivities observed in this study are particularly relevant to kinetics of S−H bond cleavage in Mo_nS_{2n} clusters. Building on the chemistry and observed reactivities in this work, experimental and computational studies of the thermodynamics of S−H and S−C bonds in $Cp^*_2Mo_2S_4$ complexes are in progress and will be the subject of future publications.

Experimental Procedures

Instrumentation. Photolysis experiments were run using a 1-kW Hanovia high pressure xenon arc lamp, and samples were prepared in degassed benzene or benzene-d_6 in Pyrex tubes. ^{1}H NMR spectra were acquired using a Varian Inova 500 or VXR-300 spectrometer, and the chemical shifts were referenced to TMS using the residual solvent peak as a secondary reference (1.94 ppm for acetonitrile-d_3, 2.09 ppm for toluene-d_8, and 7.15 ppm for benzene-d_6). EPR spectra were recorded using a Bruker EMX 9 GHz spectrometer with g values measured relative to solid DPPH ($g = 2.0036$). Magnetic susceptibilities were determined by the solution NMR method developed by Evans.[44,45] Electrospray ionization (ESI) mass spectra were collected using a Thermo Finnigan TSQ 7000 or an in-house-developed 11.5 T FTICR MS.[51] GC analyses were carried out using a Hewlett−Packard 5890 Series II GC equipped with a splitless injector and a 30 m × 0.25 mm DB-5 high performance capillary column and a flame-ionization detector. Elemental analyses were performed by Desert Analytics in Tucson, Arizona.

Electrochemical data were collected using a CH Instruments model 660C computer-aided three-electrode potentiostat in either acetonitrile or THF with 0.3 M tetraethylammonium tetrafluoroborate or tetrabutylammonium tetrafluoroborate, respectively. For cyclic voltammetry, the working electrode was a glassy carbon disk, the counter electrode was a glassy carbon rod, and a silver chloride coated silver wire was used as a pseudoreference electrode and was separated from the main compartment by a Vycor disk (1/8 in. diameter) obtained from Bioanalytical Systems, Inc. Ferrocene or decamethylferrocene was used as an internal reference with all potentials reported versus the ferrocene/ferrocenium couple. In bulk electrolysis experiments, the working electrode was a 1.2-cm diameter, 2.5-cm tall cylindrical piece of 30 pore per inch reticulated vitreous carbon purchased from ERG. The counter electrode was a 3 mm graphite rod purchased from Alfa-Aesar, and a silver chloride coated silver wire was used as a pseudoreference electrode and was separated from the main compartment by a 7-mm Vycor disk purchased from Princeton Applied Research (Cat. No. G0070).

Materials. Reagents were purchased commercially and used without further purification unless otherwise specified. All reactions, syntheses, and manipulations of Mo_2S_4 complexes were carried out under nitrogen using standard Schlenk techniques or in a glovebox. All of the preparative chromatographic separations were run using silica gel. Solvents were dried by activated alumina column in an Innovative Technology, Inc., PureSolv system or by distillation from calcium hydride (acetonitrile) or sodium and benzophenone (THF). NMR solvents were distilled from calcium hydride or dried over activated sieves, degassed, and stored in a glovebox. Benzene for photolysis experiments was triply fractionally distilled to reduce trace toluene to $\sim 10^{-7}$ M. Dibenzyl ketone (DBK) was recrystallized from methanol. **S_4H_2** was synthesized from $[Cp^*Mo(CO)_2]_2$ by the literature methods[7,9] and purified by column chromatography using dichloromethane. A new synthetic route to **S_4** is described below, and the spectroscopic data matches the previously reported data.[9] Additionally, the triflate salt of **S_4Me^+** shows very similar spectral data to the previously reported iodide analog, [Cp*Mo(μ-SMe)(μ-S)(μ-S_2)MoCp*](I).[11]

Synthesis of Cp*Mo(μ-S_2)(μ-S)$_2$MoCp*, S_4. S_4H_2 (0.75 g, 1.3 mmol) was dissolved in 100 mL of dichloromethane, and trifluoroacetic acid (0.40 mL, 5.4 mmol) was added, resulting in a color change from red to violet. After stirring overnight, triethylamine (0.75 mL, 5.4 mmol) was added, changing the solution from violet to blue. The solvent was removed, and the solid was then purified by column chromatography using 9:1 toluene and diethyl ether. Yield: 0.45 g, 60%. ^{1}H NMR (CD_3CN, 500 MHz): δ 2.13 (s, *Cp**).

Synthesis of [Cp*Mo(μ-SMe)(μ-S)(μ-S_2)MoCp*](OTf), S_4Me^+. Methyl trifluoromethane sulfonate (0.043 mL, 0.38 mmol) was added to a solution of **S_4** (0.22 g, 0.38 mmol) in 20 mL toluene. The solution changed from blue to red-brown, was stirred for 10 min, and the solvent was evaporated. The solid was purified by column chromatography with 1:4 acetonitrile and toluene to remove a yellow-brown fraction, followed by elution with acetonitrile to give a purple fraction. Yield: 0.215 g, 75%. Anal. Calcd for $C_{22}H_{33}S_5O_3F_3Mo_2$: C, 35.01; H, 4.41. Found: C, 35.35; H, 4.31. ^{1}H NMR (CD_3CN, 500 MHz): δ 2.30 (s, 30.0 H, *Cp**), 1.36 (s, 2.9 H, S*CH$_3$*). MS (*m*/*z*, ESI positive ion): 605.95 (S_4Me^+). CV, $E_{1/2}$, V (in acetonitrile): −0.93 V ($\Delta E_p = 59$ mV), −1.30 V ($\Delta E_p = 62$ mV) at 0.5 V/s. CV, $E_{1/2}$, V (in THF): −0.89 V ($\Delta E_p = 109$ mV), −1.50 V ($\Delta E_p = 110$ mV) at 0.5 V/s. Crystals suitable for X-ray diffraction were grown by slow diffusion of pentane into a toluene solution of **S_4Me^+** at room temperature under nitrogen.

Synthesis of Cp*Mo(μ-S)$_2$(μ-SMe)(μ-SH)MoCp*, S_4MeH. Methyllithium (0.20 mL of 1.6 M in diethyl ether, 0.32 mmol) was added to a solution of **S_4** (0.14 g, 0.24 mmol) in 30 mL benzene, changing the blue solution to purple. The solution was stirred for 30 min and then acetic acid (18 μL, 0.31 mmol) was added, resulting

(50) Wayner, D. D. M.; Parker, V. D. *Acc. Chem. Res.* **1993**, *26*, 287–294.
(51) Harkewicz, R.; Belov, M. E.; Anderson, G. A.; Pasa-Tolic, L.; Masselon, C. D.; Prior, D. C.; Udseth, H. R.; Smith, R. D. *J. Am. Soc. Mass Spectrom.* **2002**, *13*, 144–154.

in a red solution that was stirred for 1 h, and then the solvent was removed under vacuum. The solid was purified by column chromatography using benzene, yielding a mixture of methylated and protonated Mo_2S_4 complexes. This mixture was separated by preparative TLC using 1:4 dichloromethane and benzene, giving an approximately 1:5:5 ratio of **S_4H_2**, **S_4MeH**, and **S_4Me_2**. Yield: 0.065 g, 44%. Anal. Calcd for $C_{21}H_{34}S_4Mo_2$: C, 41.58; H, 5.65; S, 21.1. Found: C, 41.65; H, 5.59; S, 20.4. ^{1}H NMR (CD_3CN, 500 MHz): δ 2.20 (s, 30.0 H, *Cp**), 1.07 (s, 1.0 H, S*CH*$_3$, isomer B), 0.99 (s, 1.8 H, S*CH*$_3$, isomer A) −2.33 (s, 0.3 H, S*H*, isomer B), −2.51 (s, 0.6 H, S*H*, isomer A). MS (*m*/*z*, ESI positive ion): 605.95 (S_4Me^+).

Synthesis of Cp*Mo(μ-S)$_2$(μ-SMe)(μ-SBz)MoCp*, S_4MeBz. Benzylmagnesium chloride (0.040 mL of 2.0 M in THF, 0.080 mmol) was added to a solution of **S_4Me^+** (0.058 g, 0.077 mmol) in 20 mL of THF. The resulting red-orange solution was stirred for 30 min, filtered through a plug of glass wool, and the solvent was removed under vacuum to give a red solid. Yield: 0.042 g, 77%. Anal. Calcd for $C_{28}H_{40}S_4Mo_2$: C, 48.27; H, 5.79; S, 18.4. Found: C, 48.74; H, 5.51; S, 18.6. ^{1}H NMR (C_6D_6, 500 MHz): 7.08 (t, 2.2 H, Ar*H*), 7.03 (t, 2.0 H, Ar*H*), 6.94 (d, 0.9 H, Ar*H*), 2.82 (s, 0.1 H, S*CH*$_2$Ph, isomer B), 2.78 (s, 1.9 H, S*CH*$_2$Ph, isomer A), 2.16 (s, 27.6 H, *Cp**, isomer A), 2.14 (s, 2.4 H, *Cp**, isomer B), 1.14 (s, 0.2 H, S*CH*$_3$, isomer B), 1.00 (s, 2.8 H, S*CH*$_3$, isomer A). Crystals suitable for X-ray diffraction were grown from a benzene solution of **S_4MeBz** by slow evaporation at room temperature under nitrogen.

Synthesis of (Cp*Mo(μ-S)$_2$(μ-SMe)MoCp*)$_2$(μ-S_2), $(S_4Me)_2$. Method 1: Chemical Reduction. **S_4Me^+** (0.215 g, 0.285 mmol) and bis(benzene)chromium (0) (0.058 g, 0.279 mmol) were stirred in 15 mL of acetonitrile for 5 h. The resulting purple precipitate was collected by filtration, dried under vacuum, and used without purification. Yield: 0.155 g, 92%. Anal. Calcd for $C_{21}H_{33}S_4Mo_2$: C, 41.65; H, 5.49; S, 21.2. Found: C, 40.56; H, 5.40; S, 20.8. Subsequent analyses of the same sample with time resulted in progressively lower values, suggesting the sample was highly reactive, as per discussions with Desert Analytics. MS (*m*/*z*, ESI positive ion): 605.95 (**S_4Me^+**). CV, $E_{1/2}$, V (in THF): −0.90 V (ΔE_p = 96 mV), −1.49 V (ΔE_p = 102 mV) at 0.5 V/s. Crystals suitable for X-ray diffraction were grown by slow diffusion of acetonitrile into a toluene solution of **$(S_4Me)_2$** at room temperature under nitrogen.

Method 2: Bulk Electrolysis. In a typical experiment, **S_4Me^+** (0.037 g, 0.049 mmol) was dissolved in 0.3 M tetraethylammonium tetrafluoroborate in acetonitrile and reduced by constant potential electrolysis at −1.06 V vs $FeCp_2$ (100 mV negative of the peak for the reduction wave), passing 3.9 C (4.3 C was expected for a one electron reduction). The resulting precipitate was collected by filtration and washed with minimal acetonitrile to remove electrolyte. Spectroscopic data matched the product of method 1.

Magnetic Susceptibility of $(S_4Me)_2$. A solution of **$(S_4Me)_2$** (0.018 M in toluene at 26 ± 1 °C) was used to determine the magnetic susceptibility by the Evans method using ^{1}H NMR.[44,45] The solution was transferred into a 5-mm NMR tube with a sealed capillary of pure toluene. Only one methyl peak could be observed for toluene (3 Hz line width), whereas two would be expected for a paramagnetic sample at this concentration.

EPR of $(S_4Me)_2$. EPR spectra were collected for **$(S_4Me)_2$** in toluene at three concentrations (0.016, 0.0041, and 0.0011 M at 23 ± 3 °C): g = 2.003. TEMPO (8.4×10^{-5} M) was run in the same EPR tube in a separate experiment, and the data for TEMPO and **$(S_4Me)_2$**/**$S_4Me\cdot$** were double integrated and used to determine the concentration of **$S_4Me\cdot$** in each sample. The data from nine experiments were combined to give $K_{dim} = 5.9 \times 10^4 \pm 2.3 \times 10^4$ M^{-1}, where the error is two times the standard deviation.

Variable Temperature NMR of $(S_4Me)_2$. ^{1}H NMR spectra of **$(S_4Me)_2$** were collected in toluene-d_8 at 0.006 or 0.001 M total concentration, assuming all **$(S_4Me)_2$**. At or below −33 °C, the spectrum was resolved into eight Cp* methyl singlets at 2.33, 2.32, 2.31, 2.30, 2.18, 2.16, 2.15, and 2.14 ppm integrating to a total of 30.0 H (with the peaks at 2.32 and 2.14 having twice the area of the other six). Methane thiolate peaks were observed at 1.00 ppm (singlet, 1.8 H), and 0.75 ppm (two peaks, separated by 0.006 ppm, 1.1 H total). At +10 °C or higher, the methane thiolate peaks coalesced and were no longer observable, and the Cp* methyl peaks coalesced into one broad peak that shifted downfield with increasing temperature or decreasing concentration. Above 50 °C, significant decomposition occurred within 15 min, resulting in the formation of equal amounts of **S_4Me_2** and ***anti*-S_4**, as well as additional unidentified products.

Reaction of $(S_4Me)_2$ with Hydrogen. A solution of **$(S_4Me)_2$** in toluene-d_8 was purged with H_2 (1 atm) for 5 min and then ^{1}H NMR spectra were acquired, showing 60% conversion to **S_4MeH** after 5 min and complete conversion by 30 min. No other products were observed. Similarly, a solution of **$(S_4Me)_2$** in toluene was run by EPR, purged with H_2 (1 atm) for 10 min and run again, showing loss of the EPR signal.

Rate Constants for the Reaction of Benzyl Radical with S_4MeH. Hydrogen atom abstraction kinetics were determined by the previously reported method using **S_4MeH** (1.3×10^{-4} M) as the hydrogen atom donor.[37] Benzyl radicals were produced by two second photolysis of DBK (0.02 M), and the rate of hydrogen atom abstraction was determined by competition relative to the rate of formation of bibenzyl. Rate constants were calculated using density-corrected concentrations of toluene, bibenzyl, initial S_4MeH concentration (DH) using eq 11 of Scheme 3.

Photolysis of DBK and S_4MeH for Product Analysis. A solution of **S_4MeH** (0.0015 M) and DBK (0.014 M) was photolyzed for 0 to 150 s and analyzed by ^{1}H NMR to obtain the spectra in Figure 3. The products observed were toluene, bibenzyl, phenyl acetaldehyde, **S_4MeBz**, and an additional product with Cp* resonance at 1.90 ppm. Monitoring this mixture by ^{1}H NMR for one week showed ∼75% conversion of the product at 1.90 ppm to **S_4MeBz**.

Photolysis of S_4MeBz and DBK in Benzene-d_6 To Detect Photo-Conversion. A solution of **S_4MeBz** and DBK was photolyzed for 300 s and analyzed by ^{1}H NMR. Approximately 20% of the **S_4MeBz** was converted to the product with a Cp* resonance 1.90 ppm, matching that described the photolysis of DBK and **S_4MeH**.

Photolysis of S_4MeBz in Benzene-d_6 To Detect Photo-Decomposition. A solution of **S_4MeBz** without DBK was photolyzed for 450 s and analyzed by ^{1}H NMR. The ratio of isomers A and B shifted from ∼2:1 to ∼2:3 during the photolysis. No other changes were observed.

Photolysis of S_4MeH in Benzene-d_6 To Detect Photo-Decomposition. A solution of **S_4MeH** in was photolyzed for 300 s and analyzed by ^{1}H NMR. The ratio of isomers A and B shifted from ∼2:1 to 1:1 during the photolysis. No other changes were observed.

Photolysis of $(S_4Me)_2$ in Benzene-d_6 To Detect Photo-Decomposition. A solution of **$(S_4Me)_2$** was photolyzed for 250 s and analyzed by ^{1}H NMR. No changes were observed.

Single Crystal X-ray Diffraction. Crystals of **S_4Me^+**, **S_4MeBz**, and **$(S_4Me)_2$** were removed from the flask, a suitable crystal was selected, attached to a glass fiber and data were collected at 90(2) K using a Bruker/Siemens SMART APEX instrument (Mo Kα radiation, λ = 0.71073 Å) equipped with a Cryocool NeverIce low temperature device. Data were measured using omega scans 0.3° per frame for 30, 30, and 5 s respectively, and a full sphere of data was collected for all. A total of 2400 frames were collected with a final resolution of 0.83 Å. Details of the data collections and refinements are given in Table 5. Further details are provided in the Supporting Information.

S_4Me^+. Cell parameters were retrieved using SMART software.[52] The data were rotationally twinned and were deconvoluted using CELL_NOW,[53] giving a two component twin relationship: 2° rotation about the reciprocal axis −0.959, −0.127, 1.000, with

Table 5. Crystal Data and Refinement Parameters for **S_4Me^+**, **S_4MeBz**, and **$(S_4Me)_2$**

complex	S_4Me^+	S_4MeBz	$(S_4Me)_2$
formula	$C_{47.50}$ H_{70} F_6 Mo_4 O_6 S_{10}	C_{34} H_{46} Mo_2 S_4	C_{42} H_{66} Mo_4 S_8
fw (amu)	1555.40	774.83	1211.19
T (K)	90(2)	90(2)	90(2)
λ (Mo Kα) (Å)	0.71073	0.71073	0.71073
crystal system	monoclinic	triclinic	tetragonal
space group	$C2/c$	$P\bar{1}$	P 41 21 2
unit cell dimensions			
a (Å)	33.703(5)	10.5202(4)	11.6316(4)
b (Å)	20.664(3)	12.5398(5)	11.6316(4)
c (Å)	23.485(4)	26.2385(10)	35.549(2)
α (deg)	90	87.631(2)	90
β (deg)	132.887(2)	84.018(2)	90
γ (deg)	90	78.866(1)	90
volume (Å^3)	11984(3)	3377.0(2)	4809.6(4)
Z	8	4	4
ρ, calcd (Mg/m^3)	1.724	1.524	1.673
μ, (mm^{-1})	1.229	1.012	1.396
F(000)	6280	1592	2456
crystal size (mm^3)	0.54 × 0.08 × 0.04	0.28 × 0.14 × 0.06	0.33 × 0.24 × 0.11
crystal color and habit	red needle	red fragment	red plate
θ range	1.65 to 25.25°	1.81 to 25.25°	1.84 to 25.25°
index ranges	$-40 \le h$′29	$-12 \le h \le 12$	$-13 \le h \le 13$
	$0 \le k \le 24$	$-15 \le k \le 15$	$-13 \le k \le 13$
	$0 \le l \le 28$	$-31 \le l \le 31$	$-42 \le l \le 42$
reflections collected	136982	48347	68317
independent reflections	26319 [R(int) = 0.0000]	12243 [R(int) = 0.0326]	4348 [R(int) = 0.0361]
completeness to theta = 25.25°	99.9%	100.0%	100.0%
max. and min. transmission	0.9525 and 0.5565	0.9417 and 0.7647	0.8616 and 0.6559
data/restraints/parameters	26319/7/675	12243/7/764	4348/1/286
goodness-of-fit on F^2	0.966	1.048	1.059
final R^a indices	$R1$ = 0.0651,	$R1$ = 0.0362,	$R1$ = 0.0249,
[$I > 2\sigma(I)$]	w$R2$ = 0.1555	w$R2$ = 0.0774	w$R2$ = 0.0604
largest diff. peak and hole (e$^-$/Å^3)	2.950 and −1.899	0.758 and −0.532	0.764 and −0.453

[a] $R_1 = \Sigma||F_o| - |F_c||/\Sigma|F_o|$; $wR_2 = \{\Sigma[\ w(F_o^2 - F_c^2)^2]/\Sigma\ [w(F_o^2)^2]\}^{1/2}$.

a refined twinning ratio of 0.2769(5). The matrix used to relate the second orientation to the first domain is: 1.004, 0.041, 0.009, −0.029, 0.999, −0.028, −0.005, −0.001, 0.995. Each cell component was refined using SAINTPlus[54] on all observed reflections. Data reduction and correction for Lp and decay were performed using the SAINTPlus software. Absorption corrections were applied using TWINABS.[55] The structure was solved by direct methods and refined by least-squares method on F^2 using the SHELXTL program package.[56] The structure was solved in the space group $C2/c$ (#15) by analysis of systematic absences. One triflate group is disordered and was modeled in two positions with occupancies of 57/43% using restraints. Only the sulfur atom was refined anisotropically. The toluene solvent molecule was modeled using rigid coordinates, held isotropic with 50% occupancy. The sulfur bridges in the Mo3/Mo4 unit were disordered and modeled in two positions with occupancies of 87/13% (S5, S6, S7) and refined anisotropically with restraints. All other non-hydrogen atoms were refined anisotropically. No decomposition was observed during data collection.

S_4MeBz. Cell parameters were retrieved using SMART software[52] and refined using SAINTPlus[54] on all observed reflections. Data reduction and correction for Lp and decay were performed using the SAINTPlus software. Absorption corrections were applied using SADABS.[57] The structure was solved by direct methods and refined by least-squares method on F^2 using the SHELXTL program package.[56] The structure was solved in the space group $P\bar{1}$ (#2) by analysis of systematic absences. All non-hydrogen atoms were refined anisotropically. The central sulfur system is disordered with the two positions for the S, Me, and methylene groups as well as one benzyl group (89:11% occupancy). Soft restraints were applied to the minor component to stabilize geometry. No decomposition was observed during data collection.

$(S_4Me)_2$. Cell parameters were retrieved using SMART software[52] and refined using SAINTPlus[54] on all observed reflections. Data reduction and correction for Lp and decay were performed using the SAINTPlus software. Absorption corrections were applied using SADABS.[57] The structure was solved by direct methods and refined by least-squares method on F^2 using the SHELXTL program package.[56] The structure was solved in the space group P4(1)2(1)2 (#92) by analysis of systematic absences. The FLACK parameter was refined using TWIN/BASF resulting in a value of 0.00(5). The central sulfur atoms S1−S4 were disordered 50% in the first moiety and 50% for S1b, S2b, and S4b. S3 was further disordered into two positions, S3b and S3c, at 25% occupancy each. The disordered methyl groups were site refined to give C21a, 50%, and C21b, C21c, 25%. There are several close inter $X...Y$ contacts due to this disorder which implies disorder of the Cp* ring. As the SMe disorder is 25%, further disorder modeling of the Cp* methyl groups was not pursued. Disordered carbon atoms as well as S3, S3b, and S3c were held isotropic. Soft restraints were applied to S−C distances. All other non-hydrogen atoms were refined anisotropically. No decomposition was observed during data collection.

Acknowledgment. This work was supported by the U.S. Department of Energy's (DOE) Office of Basic Energy Sciences, Chemical Sciences Program. The Pacific Northwest National Laboratory is operated by Battelle for DOE. The Bruker (Siemens)

(52) *SMART*: v. 5.632, Bruker AXS: Madison, WI, 2005.
(53) Sheldrick, G. M. *CELL_NOW*: 2002.
(54) *SAINTPlus*: v. 7.23a, Data Reduction and Correction Program; Bruker AXS: Madison, WI, 2004.
(55) Sheldrick, G. M. *TWINABS*: v.1.05, an empirical absorption correction program, Bruker AXS, Inc.: Madison, WI, 2002.
(56) Sheldrick, G. M. *SHELXTL*: v. 6.14, Structure Determination Software Suite, Bruker AXS, Inc.: Madison, WI, 2004.
(57) *SADABS*: v. 2004/1, an empirical absorption correction program, Bruker AXS, Inc.: Madison, WI, 2004.

SMART APEX diffraction facility was established at the University of Idaho with the assistance of the NSF-EPSCoR program and the M. J. Murdock Charitable Trust, Vancouver, WA, USA. The authors thank Blandina Valenzuela and Rui Zhang for analysis of samples by ESI−MS.

Supporting Information Available: Tables of kinetic data, details of the dynamic NMR simulations, and additional crystallographic figures, as well as X-ray data collection, refinement results, atomic coordinates, anisotropic displacement parameters, and complete bond distances and angles in CIF format for $\mathbf{S_4Me^+}$, $\mathbf{S_4MeBz}$, and $\mathbf{(S_4Me)_2}$. This material is available free of charge via the Internet at http://pubs.acs.org.

JA078115R